Searching for optimal mitigation geometries for laser resistant multilayer high reflector coatings

S. R. Qiu, J. E. Wolfe, A. M. Monterrosa, M. D. Feit, T. V. Pistor, C. J. STolz

February 28, 2011

Disclaimer

This document was prepared as an account of work sponsored by an agency of the United States government. Neither the United States government nor Lawrence Livermore National Security, LLC, nor any of their employees makes any warranty, expressed or implied, or assumes any legal liability or responsibility for the accuracy, completeness, or usefulness of any information, apparatus, product, or process disclosed, or represents that its use would not infringe privately owned rights. Reference herein to any specific commercial product, process, or service by trade name, trademark, manufacturer, or otherwise does not necessarily constitute or imply its endorsement, recommendation, or favoring by the United States government or Lawrence Livermore National Security, LLC. The views and opinions of authors expressed herein do not necessarily state or reflect those of the United States government or Lawrence Livermore National Security, LLC, and shall not be used for advertising or product endorsement purposes.

Searching for optimal mitigation geometries for laser resistant multilayer high reflector coatings

S. Roger Qiu[a*], Justin E. Wolfe[a], Anthony M. Monterrosa[b], Michael D. Feit[a],

Thomas V. Pistor[c], Christopher J. Stolz[a]

[a]Lawrence Livermore National Laboratory, 7000 East Avenue, Livermore, CA 9455. Phone:

(925) 422-1636 Fax: (925) 423-0792

[b]Department of Nuclear Engineering and Department of Materials Science & Engineering,

University of California, Berkeley, CA 94704

[c]Panoramic Technology Inc., 2039 Shattuck Ave., Suite 404, Berkeley, CA 94704

*Corresponding author: e-mail address: qiu2@llnl.gov

Growing laser damage sites on multilayer high reflector coatings can limit mirror performance. One of the strategies to improve laser damage resistance is to replace the growing damage sites with pre-designed benign mitigation structures. By mitigating the weakest site on the optic, the large aperture mirror will have a laser resistance comparable to the intrinsic value of the multilayer coating. To determine the optimal mitigation geometry, the finite difference time domain method (FDTD) was used to quantify the electric-field intensification within the multilayer, at the presence of different conical pits. We find that the field intensification induced by the mitigation pit is strongly dependent on the polarization and the angle of incidence (AOI) of the incoming wave. Therefore the optimal mitigation conical pit geometry is application specific. Furthermore, our simulation also illustrates an alternative means to achieve an optimal

mitigation structure by matching the cone angle of the structure with the AOI of the incoming wave, except for the p-polarization wave at a range of incident angles between 30° and 45°.

OCIS codes: (310.0310) Thin film, (230.7370) Waveguide, (140.3330) Damage.

1. Introduction

High-dielectric constant multilayer coatings are commonly used on mirrors for high-peak power laser systems because of their high laser damage resistance. For example, in mirrors used in the National Ignition Facility, silica-hafnia multilayer coatings are coated on BK7 substrates by e-beam physical vapor deposition. During the deposition process, physical defects are often formed within the multilayer film. These physical defects include highly absorbing nano-clusters at the near surface region of the film and solid inclusions in the bulk film. In addition, some substrate surface flaws (e.g. scratches) can also cause films to grow defectively. Earlier studies [1-4] have shown that all these defect types can cause laser-induced damage in the coated layers even at a fluence that is much lower than that of the operating fluence. Some of these initiated damage sites, although rare in comparison to the total number of defects within the film, can grow under further laser irradiation, and thus eventually limit the mirror performance and lifetime.

In parallel with attempts to increase film quality by suppressing the number of defects within the coating layers, other active efforts have also been made to enhance mirror performance and lifetime by increasing the damage threshold upon laser irradiation. One of the strategies is to first initiate the damage precursors at fluencies below the operational fluence and then replace the initiated damage sites with a pre-designed benign mitigation structure [5] with a much higher

damage threshold. These mitigation structures can be created by multiple techniques including femtosecond laser machining, single crystal high-speed diamond machining, and magnetorheological finishing [5-7]. In fact, our earlier study of creating rationally designed features utilizing femtosecond laser machining [5] has shown an increase in the laser damage threshold, from 15 J/cm^2 to 40 J/cm^2 for light at 1064 nm, with a 3ns pulse length. However, to maximize the effort, one must have a rational means to search for an optimal mitigation structure that can routinely yield a higher laser damage threshold than the operational fluence.

A combination of theoretical and experimental efforts has been put forth to determine the optimal mitigation geometry. For the theoretical effort, we have utilized the FDTD method to quantify the electric-field distribution within the coating layers in the presence of the pre-defined defects of different shapes. This approach is motivated by the fact that laser-induced damage within thin film layers is strongly correlated with electric field intensification due to interference between incident beam and secondary waves created by the presence of thin film interfaces and coating defects [8-11]. Experimentally, we utilize femtosecond laser machining to fabricate mitigation structures suggested by the simulation work and to further examine the manufactured feature for damage resistance as well as to validate the theoretical predication.

In this paper, we report on results examining conical pits as potential mitigation geometries. To realistically mimic the true mitigation features, the theoretical simulation was performed as a 3-D structure with cone angles ranging from 0° to 75° in 15° increments and the laser beam incidence angles of 0° to 60° in 5° increments. Furthermore, the impact of polarization on multilayer laser damage resistance was also investigated. Overall, results of electric-field intensification

obtained through 3-D simulation are consistent with those obtained previously through 2-D simulation [12]. For a conical pit-bearing multilayer coating, the light intensification within the coating layers is generally smaller for pits with cone angles less than 30º. This is true for both hafnia and silica layers at either s or p polarizations. Alternatively, for the hafnia layer, the field intensification can be minimized when the cone angle matches the incident angle of s polarized light. For p polarized light, similar results hold for those angles that are either smaller than 25° or greater than 45°. The simulation results are consistent with experimental observation through laser-induced damage testing. Previous studies have shown that laser-induced damage within multilayer coatings usually occurs in the high-index layer such as hafnia [13-14]. Utilization of the design strategy for non-quarter wave high reflector by suppressing electric-field in high dialectic constant layer while neglecting the increase of electric-field in the lower index layer has demonstrated the improved laser damage resistance [13]. Based our the simulation results over the hafnia layer, we suggest that conical pits can be used as potential mitigation structures, as long as the cone angle satisfies the criteria for the specific application as summarized in table 1, or the cone angle matches with the application AOI except for the p-polarization wave at incident angles between 30° and 45°.

2. Method

A commercially available software code TEMPESTpr2 employing the FDTD method is used to solve Maxwell's equations within a 3-D domain containing conical pit structures. A detailed description of this code can be found elsewhere [15]. For the current application, the algorithm simulates the scattering of an electromagnetic plane wave that propagates through a defective multilayer topography as shown in Fig. 1. The simulation domain is a 3-D rectangular and

gridded uniformly. The periodic boundary conditions (PBC) are applied in the horizontal direction, while the Berenger's perfectly matched layer (PML) absorbing-boundary condition is applied in the vertical direction. In addition, absorbing layers with median refractive indices were also manually added to the outside edges of the simulation domain in the x-z plane to minimize the impact of the PBC and to prevent back reflections. The validation of the application of this code for calculating electric-field intensification for a multilayer high reflector coating is discussed in detail in reference [12].

The 3-D domain used for the current study (Fig. 1) consists of twenty-four alternating layers of hafnia (H) and silica (L) with a quarter-wave reflector design: air:L(L:H)^12:glass. The refractive indices of the layers are n_H=1.971 and n_L=1.44977. The physical thickness of each hafnia and silica layer is 133.56 and 181.58 nm, respectively. The total film thickness is 3963.26 nm. Due to the limitation of computation power for the 3-D simulations, the film thickness is discretized with a 7-cell per bilayer instead of the 12-cell per bilayer arrangement for the 2-D calculation [12]. For conical pits, the cone angles range from 0° to 75° at 15° increments and the incident angles of the incoming wave range from 0° to 60° at 5° increments. For oblique incidence cases, the irradiation wavelength for the simulation was blue-shifted to maintain maximum reflectivity and proper spectral centering; the refractive indices were also replaced by the effective values to ensure the quarter wave optical thickness is satisfied throughout the simulations. The description of film thickness, wavelength, and refractive index modifications for waves impinged along off-normal directions can be found in detail in ref. [12]. The electric-field intensification strength within the domain is quantified by the normalized electric-field intensity or the square of electric field, $|\mathbf{E}|^2$ with respect to that of the incoming wave; i.e., a

value of 1 indicates no field intensification and the larger the value, the stronger the electric-field intensification.

Femtosecond laser machining is used to create conical pits of 15º on a 2" round BK 7 substrate [5] coated with high reflective multilayer similar to those used in the simulations. The pits are created with diameters of 0.51.0 mm and are ~10-15 um deep. To validate the simulation prediction of maximum electric-field intensification and the possible laser-induced damage region, the mitigation feature-bearing multilayer film is examined for laser-induced damage by following a standard damage testing protocol in reference [16] . In summary, a 1064 nm, 3 ns laser with a 1 mm Gaussian spot at $1/e^2$ is raster scanned in approximately 200 μm steps across the test area of 1 cm^2. The test scan starts at a low fluence of 1.0 J/cm^2 and ramps up in 3.0 J/cm^2 increments until damage is observed. The damage fluence is defined as the lowest fluence at which any growing sites are observed.

3. Results and Discussion

Simulation results show that electric-field intensification exists in both hafnia and silica layers for multilayer coating that contains conical pits. Because the damage resistance and the correlation between light intensification and damage initiation or growth of these materials are different, the simulation results are grouped by material type; i.e., hafnia and silica. The characteristics of electric-field intensification within the hafnia layers are shown in Figs. 2-5 and those within the silica layers are shown in Figs. 6-9. In general, for both material types, the spatial distribution of the electric-field intensification is polarization-dependent and the

maximum intensification is in the opposite side of the cone for s- and p-polarized light, respectively. This is true for all cone angles and angles of incidence.

It should be noted that the reported domain size is the largest dimension of an isolated site that we can simulate accurately and also the closest size to the practical mitigation structure. The multilayer design was selected for practical purposes. Since no simulations were done on larger domains and pits, nor with other types of multilayer design, it is uncertain how the results scale. The dependence of the maximum field intensification within the multilayer coating on pit cone angle, however, does provide a general trend of the system at any scale.

3.1 Electrical field intensification within the hafnia layers

The cross-sectional view of the electric-field intensification distribution within the multilayer coating is shown in Figs. 2 and 3 for both s- and p-polarized waves at the presence of a conical pit of 15º. When the s wave is irradiated at 45º off-normal to the left, the high intensification area is manifested at the right side region to the cone. However, for p-polarized light, the high intensification region is at locations on the left side of the cone. Such a difference can be easily discerned in Figs. 2 and 3. While Figs. 2 (a) and 3 (a) show the top-view of the electric-field intensification at the layer where maximum intensification resides, Figs. 2 (b) and 3 (b) show the side view of the field intensification within the film. The higher the color scale is, the larger the field enhancement. The maximum intensification for the s wave is located at the second hafnia layer from the top, but for the p wave, it is located at the top layer. The maximum intensification spot for both cases is shown by the red spot in Figs. 2 (b) and 3 (b), respectively.

To understand the general trend of the electric-field intensification in the multilayer coating with a mitigation feature, simulations were performed for different conical pits irradiated at both s- and p-polarized light at various incident angles. The maximum intensification values under s-polarized light (s wave) are summarized in Fig. 4 for all simulated conditions. Both a column plot and a surface plot were used to better display the important features of the simulated results. As shown in Fig. 4 (a), for the s-polarized light, the maximum intensification in the hafnia layer varies in a wide range, for example from as low as 1.5 to as high as 9.5, depending on the combination of cone angle and light irradiation direction. For a given cone angle, the dependence on incident angles in most cases can be expressed by a monotonic function. However, for a fixed AOI, the dependence of the maximum intensification on cone angles is more complex and does not follow a simple trend.

To better visualize the convoluted impact of both the cone angle and AOI on electric-field intensification, the simulation results are displayed in a pseudo-3D surface plot (Fig. 4 (b). Besides displaying the information already discussed in Fig. 4(a), Fig. 4(b) shows that there are two ways to minimize the electric- field intensification within the multilayer coating due to the existence of the mitigation conical pit. For an AOI smaller than 35°, one can choose pits with conical angles between zero and 30°. For an AOI greater than 35°, the conical angle can be between 15° and 60° (see table 1). An alternative way would be matching the conical angle with the light incident angle and this approach is suitable for applications of all AOI. A solid blue line is added to the figure to guide readers.

The simulation result for the p-polarized light (p wave) is shown in Fig. 5. As shown in Fig. 5 (a) the magnitude of the maximum field intensification for all cases studied is much smaller than that for the s wave. For example, at p-polarization, for a feature at a 45°cone angle at normal incidence, the intensification maximum is only 4 compared to nearly 10 at s-polarization. The difference in the maximum intensification can be attributed in part to the nature of electrodynamic boundary condition. For the s polarization wave, the electric field of the incoming wave is parallel to the coating surface at some position. The electrical field is thus continuous when across the material boundary. The p polarization wave, on the other hand, lies within the plane of incidence but is perpendicular to the propagation direction. Therefore, only the component of the electric field parallel to the surface is continuous across the material boundary. The other component is reduced in magnitude. Subsequently, for the maximum case, the strength of the electrical field within the coating is larger for the s polarization wave than that of the p polarization wave. Overall, our results suggest that the multilayer high reflector coating may be more robust against impinging p-polarized light.

Similar to the case with s wave, the dependence of intensification on cone angle and AOI does not follow a simple trend. As indicated in Fig. 5(b), the suppression of electric-field intensification due to the introduction of mitigation pits is strongly dependent on the specific application. For application with AOI ranging from zero up to 25°, the cone angle of the optimal mitigation pit needs to be smaller than 30°. For those AOI ranging from 25° to 45°, the pit conical angle can be between 55° to 65° and for the AOI greater than 45°, one can choose a pit with cone angle from 45° up to 75° (see table 1). Alternatively, for applications with AOI

9

ranging from 0° to 25°, and from 45° to 60°, the least field intensification can be achieved by matching the pit cone angle.

3.2 Electric-field intensification within the silica layers

Simulation results for the silica layers showed very similar characteristics to that of the hafnia layers in electric-field intensification. Examples of the cross-sectional distribution of the electric-field intensification are shown in Fig. 6 for the s wave and in Fig. 7 for the p wave; both for a 15° cone under 45° irradiation off normal. For instance, the location of the maximum intensification within the silica layers is at the right side of the cone for the s wave and at the left side of the cone for p wave. This is consistent with that for the hafnia layer. The only difference, however, is that for the s wave, the maximum intensification is at the first layer from the top in contrast to that at the second layer for the hafnia material. For the p wave, both are at the top layer.

The magnitude of the intensification maximum is displayed in Fig. 8 and Fig. 9 for s and p waves respectively. In general, for the s-polarized wave, high electric-field intensification within the silica layer occurs at lower angles of incidence for pits with larger cone angles (i.e. between 40° and 60°). For example, when the multilayer is irradiated at an incidence angle of 5°, the field intensification can reach as high as 9.5 for a pit with cone angle at 45°. On the other hand, a pit with a cone angle of zero degree (cylinder) produces much smaller field amplification for all incident angles. Alternatively, as displayed by the blue line in Fig. 8(b), for pits with cone angles either smaller than 15° or greater than 35°, the electric-field intensification within the silica layer can be minimized if the incident angle is matched with the cone angle. For p-

polarized wave, the magnitude of the electric-field intensification is much smaller than that for a s wave which behaves similarly to the hafnia layers. As shown in Fig. 9(b), the high electric-field intensification is only concentrated in a small domain; that is for pits with cone angles of 45° and 60° at incidence angles smaller than 5°. Amplitude of the electric-field intensification for all the other scenarios are within or below 3. Furthermore, as indicated by the blue line in Fig. 9(b), field intensification can be minimized if one chooses a mitigation pit with cone angle smaller than 30° or that have the cone angle and the AOI matched.

In comparison to the hafnia layers, the maximum intensification within the silica layer is generally higher. However, for a given cone angle, the dependence of intensification on incident angle is not as well correlated. These characteristics are especially apparent for lower cone angles. Earlier studies have reported that laser-induced damage sites are more often initiated at the hafnia layers. Since material with less intensification is more prone to damage, our simulation results suggest that besides electric-field intensification, internal physical properties of coating materials play an important role in mirror performance.

3.3 Waveguide effect

In an earlier study, we reported our observation of an interesting phenomenon where a waveguide effect was responsible for the electric-field intensification within a defective multilayer film containing a cylinder [12]. In the current work, we conducted a thorough study by examining the waveguide effect on light intensification for a series of cones under different irradiation directions. After careful analysis of the simulation data for all combinations of cone angle and AOI, we find that the waveguide effect is the main cause of light intensification for

pits with cone angles smaller than 30° at all angles of incidence. The waveguide effect, however, is not observed to be the cause of the high intensification through the film for the p waves.

Since fabricated conical pits with cone angles smaller than 30º are one of the suggested mitigation strategies, it is beneficial to suppress the waveguide formation for the lower cone angle features. Recently, an effort has been made to create conical pits of shallower cone angles using femtosecond laser machining [5]. As a consequence of the fabrication process, the edge of the cones becomes rough with a randomly oriented serrated morphology [17]. It is speculated that a rough edge at the cone boundary may be able to break the coherence of light and thus eliminate the waveguide effect and light intensification. To test this hypothesis, preliminary simulations are performed for pits with rough edge with cone angles at 0° and 15° respectively. The input pit morphology for each simulation was derived from a digitized SEM image of the cross-section of the benign pit created by femtosecond laser machining in reference [5]. The cross-sectional view of conical pit with rough edge was achieved by a dual beam focused ion beam milling technique [18]. Fig. 10 shows the simulated field intensity distribution within the multiple layers at the presence of a 15° smooth- (Fig. 10 (a)) as well as rough-edged (Fig. 10 (b)) cone, with a light beam irradiating at 45° from the surface normal. It is apparent that a waveguide patterns exist in both cases. Thus the rough edge at the cone boundary does not reduce the waveguide effect within the film. This result suggests that the irregularity of the rough edge created by micro-machining may be too small (in comparison to the beam wavelength at 1053 nm) to reduce the coherence. Future efforts are in progress to find an effective means to suppress the waveguide effect.

3.4. Laser damage test

Laser induced-damage on multilayer coatings with different mitigation conical pits fabricated by femtosecond laser machining of various conditions has been investigated and reported in ref. [17]. Briefly, results show that mitigation features can increase the coating damage resistance by a factor of two and suggest that if the weakest laser-induced-damage-threshold site on the mirror was replaced with the mitigation feature, the local values for the specific site would far exceed the nominal damage threshold of 20 J/cm^2 for the non-mitigated multilayer high reflector coatings over large-aperture mirrors. Although the exact nature is unclear and is beyond the scope of this paper, damage precursors do definitely exist on the coating as supported by the laser damage testing results. The fact that damage sites were observed for all the experiments indicts that the damage probability is quite high around the mitigation regions, but at fluences much higher than that for typical large-aperture mirrors.

In this section, we report experimental results on a specific case employing laser testing as an example to show that the damage results agree well with our theoretical predications for both polarizations, as discussed in the previous sections (Figs. 2-3). For a multilayer coating that contain a mitigation conical pit of 15°, when irradiated the s-polarized light at 45° off the normal to the left, the thin film damage appears at a region near the mitigation site when laser fluence reaches 42 J/cm^2. For p-polarized light, the thin film damage threshold is 54 J/cm^2. Furthermore, the damaged areas under each polarization reside at the same location where the maximum electric-field intensification is predicted.

The morphology of the multilayer with the conical pit mitigation feature prior to and after damage is shown in Fig. 11. Fig. 11 (a) is a top view light microscope image that displays the features within the film. The black circle represents the conical pit and the darker fuzzy region at the upper left side of the circle is the debris from the femtosecond laser machining.   The morphology after s wave damage is shown in Fig. 11 (b). As highlighted by the yellow arrow, the film at the right side of the circle shows strong delaminations and loses its smoothness due to damage. In contrary, the damaged sites under p wave are located at the left side of the circle which can be easily seen in Fig. 11 (d) (indicated by yellow arrow). To help demonstrate the resemblance, simulation results for similar light irradiation conditions to the laser damage testing are displayed in Figs. 11 (c) and (e), for the s and p waves respectively. As indicated by the yellow circles in the figures, the predicted highest intensification spot under 45° irradiation is located at the right side of the pit for the s wave and at the left side for the p wave.

In addition to the agreement between calculations and experiment in damage locations, the fluence ratio is also comparable to the intensification ratio. For example, the theoretical calculation predicts that the maximum intensification is ~3.5 for s-polarized light and 2.6 for p-polarized light. If one assumes that the laser-induced damage is directly related to electric-field intensification, the damage threshold for the s-polarized light should be less and the measured damage threshold should be proportional to the calculated maximum intensification. This in fact is what we have observed from both the experimental testing and theoretical calculation. We find that the ratio of the maximum intensification between p and s waves is at ~ 0.74 and the ratio of measured damage fluences for s and p waves is at ~ 0.78. They are essentially the same within experimental errors. In short, the agreement between the experimental and theoretical

results further support the hypothesis that electric-field intensification is one of the major causes of laser-induced damage in multilayer high reflector coatings.

4. Summary

In summary, simulation utilizing FDTD method has shown that conical pits generate high electric-field intensification within the multilayer high reflector coating. A waveguide effect is one of the sources for field intensification, especially for mitigation features with lower cone angles. The magnitude of the intensification is strongly dependent on cone angles and the AOI of the incoming wave. The location of the maximum field intensification is also polarization dependent and the prediction has been confirmed by laser-induced damage testing. Therefore the optimal mitigation pit geometry is application specific (e.g. polarization and AOI). Based on the review of simulation results on the hafnia layer, we suggest a global mitigation strategy over the multilayer coating by fabricate conical pits with the cone angle matching with the AOI of incoming wave. Alternatively, one may choose a more application-specific approach to determine the optimal conical angle as summarized in table 1.

References

1. J. Dijon, P. Garrec, N. Kaiser, and U. B. Schallenberg, "Influence of substrate cleaning on LIDT of 355 nm HR coatings," Proc. SPIE **2966**, 178-186 (1997).
2. J. Dijon, T. Poiroux, and C. Desrumaux, "Nano absorbing centers: a key point in the laser damage of thin films," Proc. SPIE **2966**, 315-325 (1997).
3. F. Y. Genin and C. J. Stolz, "Morphologies of laser-induced damage in hafnia-silica multilayer mirror and polarizer coatings," Proc. SPIE **2870**, 439-448 (1996).
4. S. H. Li, H. B. He, D. W. Li, M. Zhou, X. L. Ling, Y. A. Zhao, and Z. X. Fan, "Temperature field analysis of TiO_2 films with high-absorptance inclusions," Appl. Opt. **49**, 329-333 (2010).
5. J. E. Wolfe, S. R. Qiu, C. J. Stolz, M. Thomas, C. Martinez, and A. Ozkan, "Laser damage resistant pits in dielectric coatings created by femtosecond laser machining," Proc. SPIE **7504**, 750405 (2009).
6. P. Geraghty, W. Carr, V. Draggoo, R. Hackel, C. Mailhiot, and M. Norton, "Surface damage growth mitigation on KDP/DKDP optics using single-crystal diamond micro-machining ball end mill contouring," Proc. SPIE **6403**, 64030Q (2007).
7. M. Tricard, P. Dumas, and J. Menapace, "Continuous phase plate polishing using magnetorheological finishing," Proc. SPIE **7062**, 70620V (2008).
8. P. W. Baumeister, *Optical Coating Technology* (SPIE, 2004).
9. C. J. Stolz, M. D. Feit, and T. V. Pistor, "Laser intensification by spherical inclusions embedded with multilayer coatings," Appl. Opt. **45**, 1594-1601 (2006).
10. Y. Wang, Y. G. Zhang, X. Liu, W. L. Chen, and Y. Y. Li, "Analysis of laser intensification by nodular defects in mid-infrared high reflectance coatings," Acta Phys. Sin. **56**, 6588-6591 (2007).
11. Y. G. Shan, H. B. He, Y. Wang, X. Li, D. W. Li, and Y. A. Zhao, "Electrical field enhancement and laser damage growth in high-reflective coatings at 1064 nm," Opt. Commun. **284**, 625-629 (2011).
12. S. R. Qiu, J. E. Wolfe, A. M. Monterrosa, M. D. Feit, T. V. Pistor, and C. J. Stolz, "Modeling of light intensification by conical pits within multilayer high reflector coatings," Proc. SPIE **7504**, 75040M (2009).
13. D. H. Gill, B. E. Newnam, and J. McLeod, "Use of non-quarter-wave-designs to increase the damage resistance of reflectors at 532 and 1064 nanometers," NBS SP **509**, 260-270 (1977).
14. S. V. Garnov, S. M. Klimentov, A. A. Said, and M. J. Soileau, "Laser damage of HR, AR-coatings, monolayers and bare surface at 1064 nm," Proc. SPIE **1848**, 162-181 (1992).
15. T. V. Pistor, "Electromagnetic simulation and modeling with applications in lithography," (University of California, Berkeley, Berkeley, 2001).
16. M. R. Borden, J. A. Folta, C. J. Stolz, J. R. Taylor, J. E. Wolfe, A. J. Griffin, and M. D. Thomas, "Improved method for laser damage testing coated optics," Proc. SPIE **5991**, 59912A (2005).
17. J. E. Wolfe, S. R. Qiu, and C. J. Stolz, "Fabrication of mitigation pits for improving laser damage resistance in dielectric mirrors by femtosecond laser machining," Appl. Opt. **Submitted**(2011).

18.   S. R. Qiu, J. E. Wolfe, A. M. Monterrosa, W. A. Steele, N. E. Teslich, M. D. Feit, T. V. Pistor, and C. J. Stolz, "Impact of substrate surface scratches on the laser damage resistance of multilayer coatings," Proc. SPIE **7842,** 78421X (2010).

Table 1: Summary of conical angle for optimal mitigation pit with minimized electric- field

intensification under different angle of incidence (AOI): (a) for S-polarization wave and (b) for

P-polarization wave.

(a)

AOI (degree)	≤ 35°	>35°
Cone angle (degree)	0°- 30°	15°- 60°

(b)

AOI (degree)	≤ 25°	25°- 45°	≥45°
Cone angle (degree)	< 30°	55°-65°	45°-75°

Figure Captions

Fig. 1. Schematics of 3-D simulation domain showing a multilayer coating with a conical pit of 15º cone angle on a BK7 glass substrate. The hafnia layers are represented by the green color while the light blue color represents silica layers, the glass substrate, and cap layer.

Fig. 2. Electrical field intensity distribution in the hafnia layer with a 15º conical pit for s-polarization light irradiated at 45º where the highest intensification resides. The maximum intensification is located at the second hafnia layer from the top and at the right side of the cone edge which is delineated by the dotted white lines. Higher color scale value corresponds to higher field enhancement. (a) Cross section (at Z = 3.69 µm) that is perpendicular to plane of incidence. (b) Cross section (at Y = 17.08 µm) that is parallel to the plane of incidence. For view purpose, the image in (b) is stretched along the vertical direction.

Fig. 3. Electrical field intensity distribution in the hafnia layer with a 15º conical pit for p-polarization light irradiated at 45º where the highest intensification resides. The maximum intensification is located at the first hafnia layer from the top and at the left side of cone edge which is delineated by the dotted white lines. Higher color scale value corresponds to higher field enhancement. (a) Cross section (at Z = 4.005 µm) that is perpendicular to plane of incidence. (b) Cross section (at Y = 42.0 µm) that is parallel to the plane of incidence. For view purpose, the image in (b) is stretched along the vertical direction.

Fig. 4. Distribution of the maximum intensification within the hafnia layers in the defective multilayer coating film for various cone angles and s-polarization light irradiation at a series of incidence angles. (a) 2-D column plot. The color-box legend indicates the angle of incidence. (b) Contour plot. The blue line indicates that light intensification in mitigation sites is minimized

when the cone angle and the incident angle are matched. The color-box legend represents the magnitude of intensification.

Fig. 5. Distribution of the maximum intensification within the hafnia layers in the defective multilayer coating film for various cone angles and p-polarization light irradiation at a series of incidence angles. (a) 2D column plot. The color-box legend indicates the angle of incidence. (b) Contour plot. The blue line indicates that light intensification in mitigation sites is minimized when the cone angle and the incident angle are matched. The color-box legend represents the magnitude of intensification.

Fig. 6. Electrical field intensity distribution in the silica layer with a 15° conical pit for s-polarization light irradiated at 45° where the highest intensification resides. The maximum intensification is located at the first silica layer from the top and at the right side of cone edge which is delineated by the dotted white lines. Higher color scale value corresponds to higher field enhancement. (a) Cross section (at Z = 4.275 μm) that is perpendicular to plane of incidence. (b) Cross section (at Y = 30.03 μm) that is parallel to the plane of incidence. For view purpose, the image in (b) is stretched along the vertical direction.

Fig. 7. Electrical field intensity distribution in the silica layer with a 15° conical pit for p-polarization light irradiated at 45° where the highest intensification resides. The maximum intensification is located at the first silica layer from the top and at the left side of cone edge which is delineated by the dotted white lines. Higher color scale value corresponds to higher field enhancement. (a) Cross section (at Z = 4.32 μm) that is perpendicular to the plane of incidence. (b) Cross section (at Y = 40.53 μm) that is parallel to the plane of incidence. For view purpose, the image in (b) is stretched along the vertical direction.

Fig. 8. Distribution of the maximum intensification within the silica layers in the defective multilayer coating film for various cone angles and s-polarization light irradiation at a series of incidence angles. (a) 2-D column plot. The color-box legend indicates the angle of incidence. (b) Contour plot. The blue line indicates that light intensification in mitigation sites is minimized when the cone angle and the incident angle are matched. The color-box legend represents the magnitude of intensification.

Fig. 9. Distribution of the maximum intensification within the silica layers in the defective multilayer coating film for various cone angles and p-polarization light irradiation at a series of incidence angles. (a) 2-D column plot. The color-box legend indicates the angle of incidence. (b) Contour plot. The blue line indicates that light intensification in mitigation sites is minimized when the cone angle and the incident angle are matched. The color-box legend represents the magnitude of intensification.

Fig. 10. Electrical field intensity distribution within multilayer coating layers at the presence of a 15° conical pit of smooth edge (a) and rough edge (b). Beam irradiated at 45° from surface normal. Domain dimension: 90 µm x 4.963 µm. For visualization purposes, all images are stretched along the vertical direction.

Fig. 11. Laser damage results on conical pits fabricated by femtosecond laser machining and its correlation to simulation results. Feature size 1 mm conical pit of 15º cone angle. (a) Light microscope image of fabricated feature before damage test. (b) Light microscope image of conical pit after testing up to 42 J/cm^2 under irradiation of 1064 nm of s-polarization laser light. (c) Simulation result showing the maximum intensification location for s-polarization light. (d) Light microscope image of conical pit after tested up to 54 J/cm^2 under irradiation of 1064 nm of

p-polarization laser light. (e) Simulation result showing the maximum intensification location

for p-polarization light.

Fig. 1.
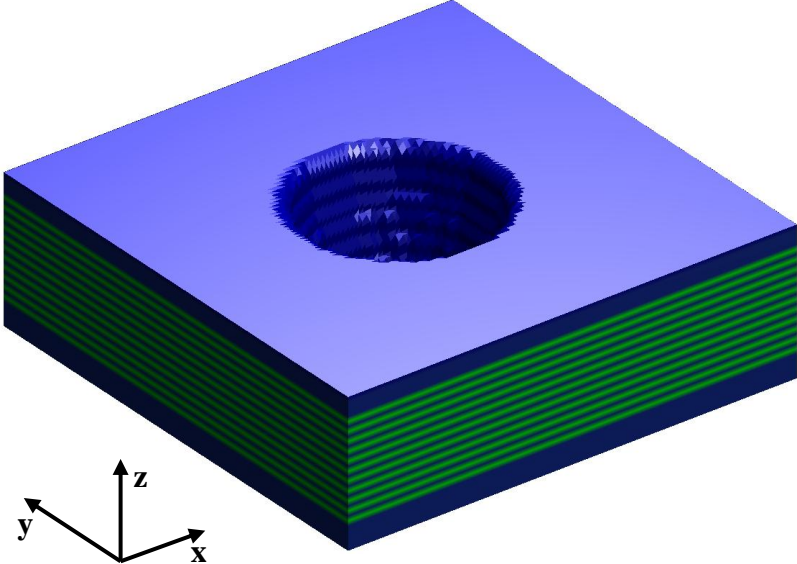
Fig. 2.

(a)
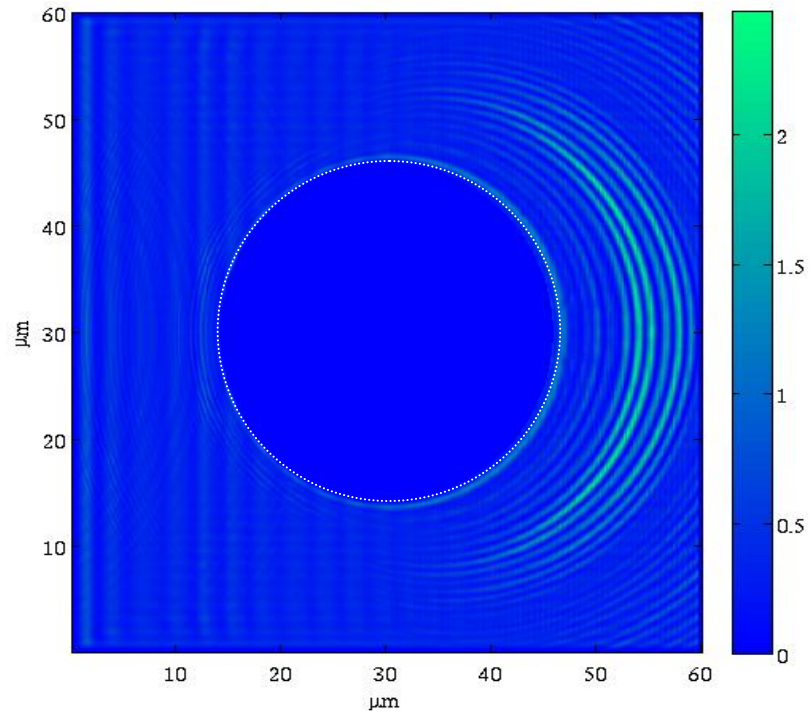
(b)
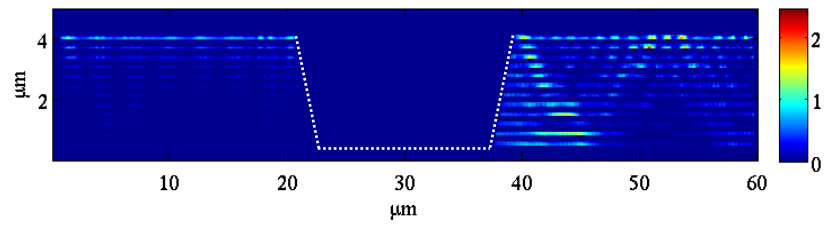
Fig. 3.

(a)
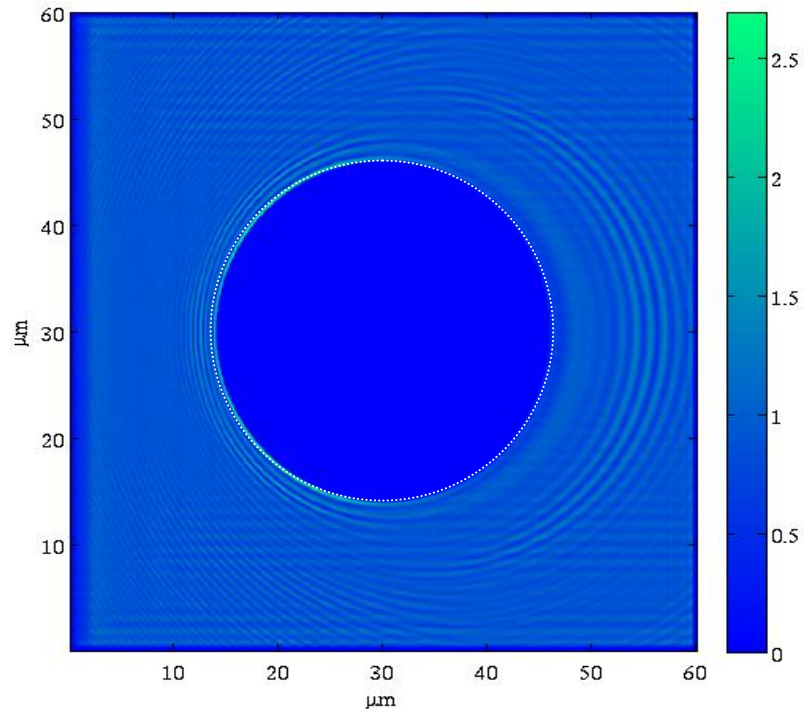
(b)
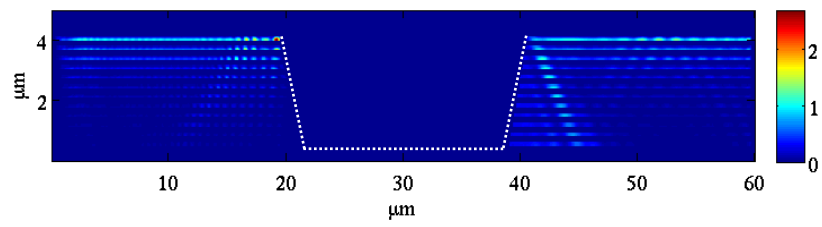
Fig. 4. (S HfOx)

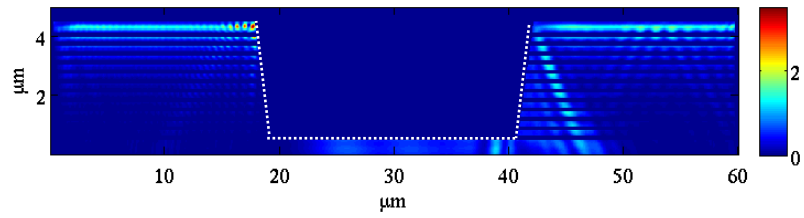**Fig. 5. (P HfOx)**

Fig. 6.

(a)

(b)
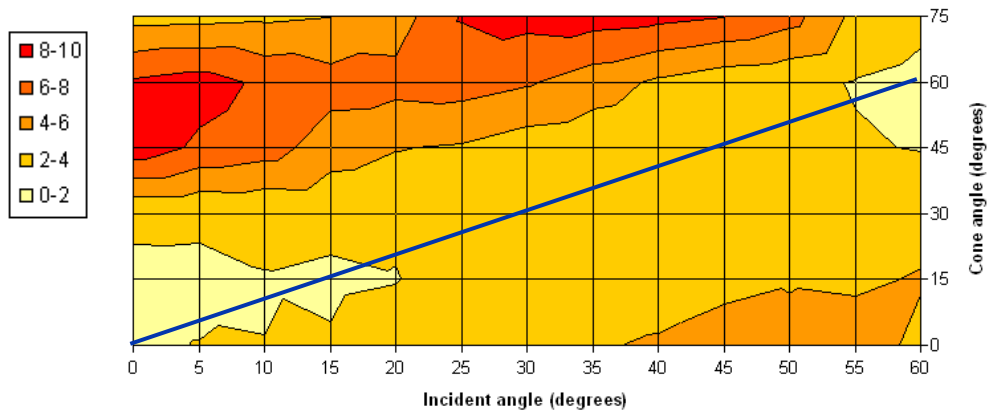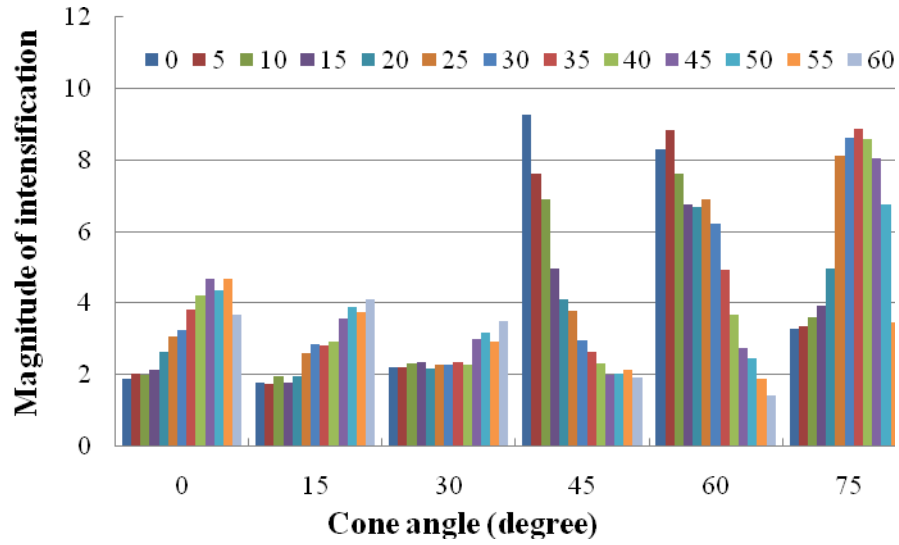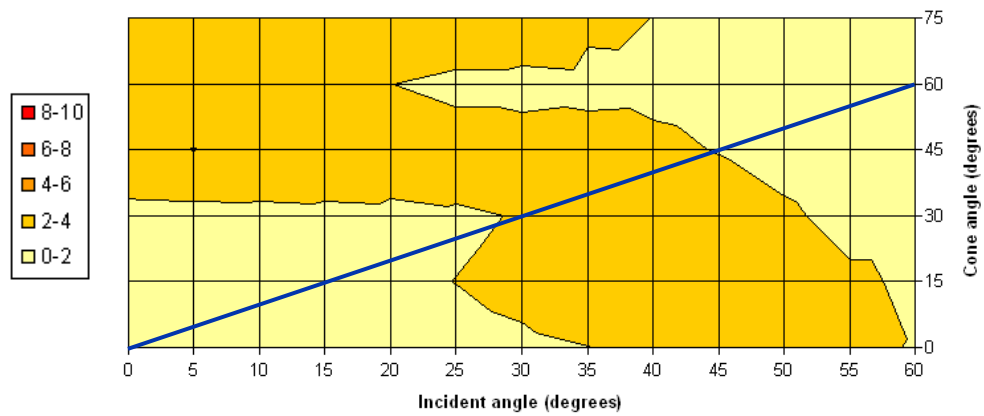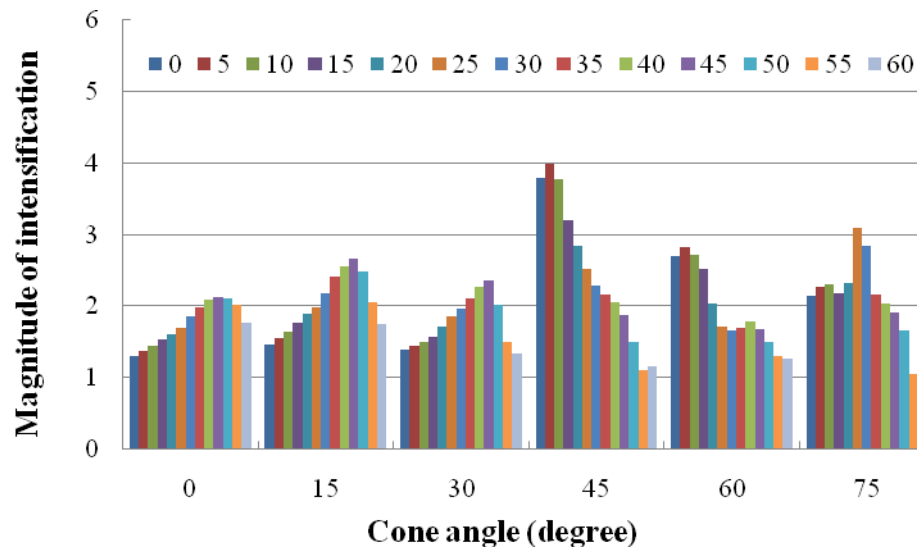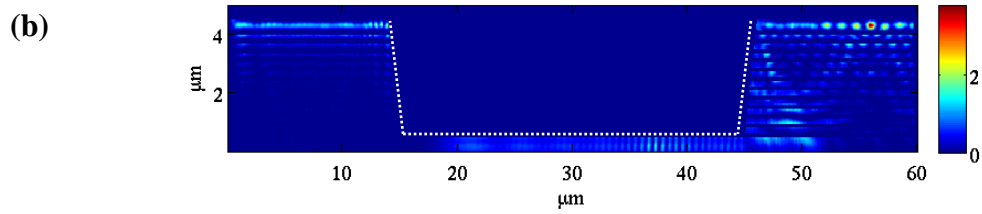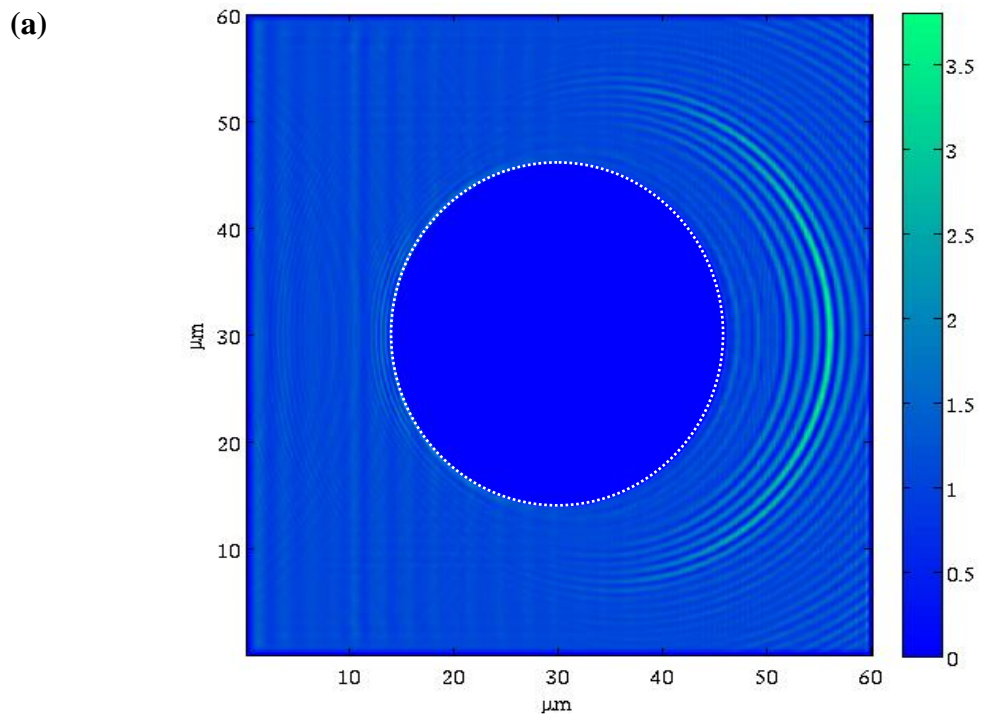
Fig. 7.

(a)
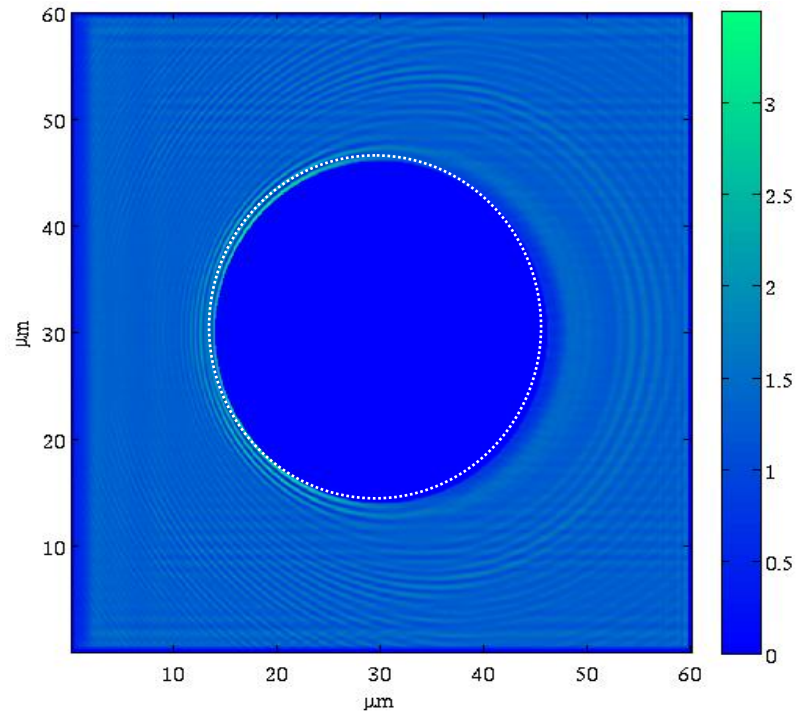
(b)

Fig. 8. (S SiOx)

Fig. 9. (P, SiOx)

Fig. 10

(a)

Intensity in All Materials (No Air) at XZ =1

(b)

Intensity in All Materials (No Air) at XZ =1

Fig. 11

(a)

(b)
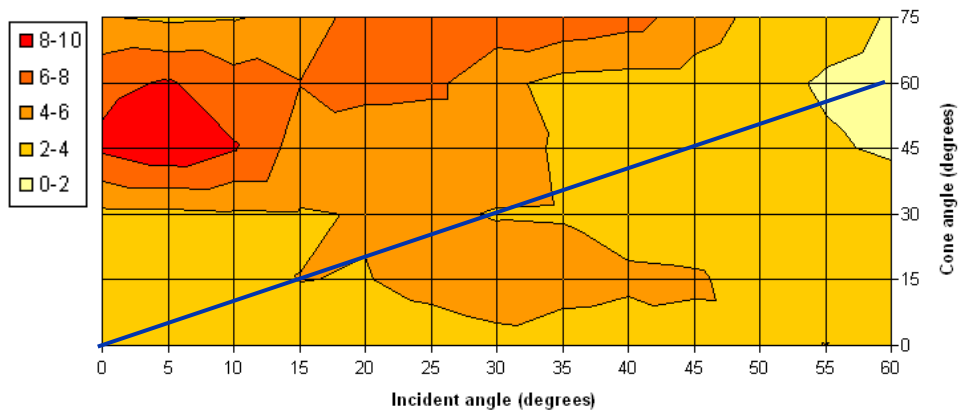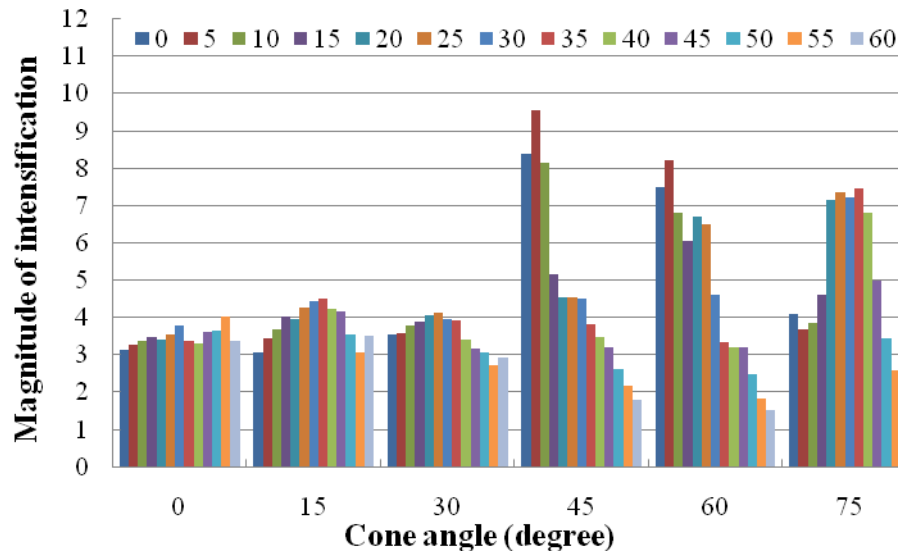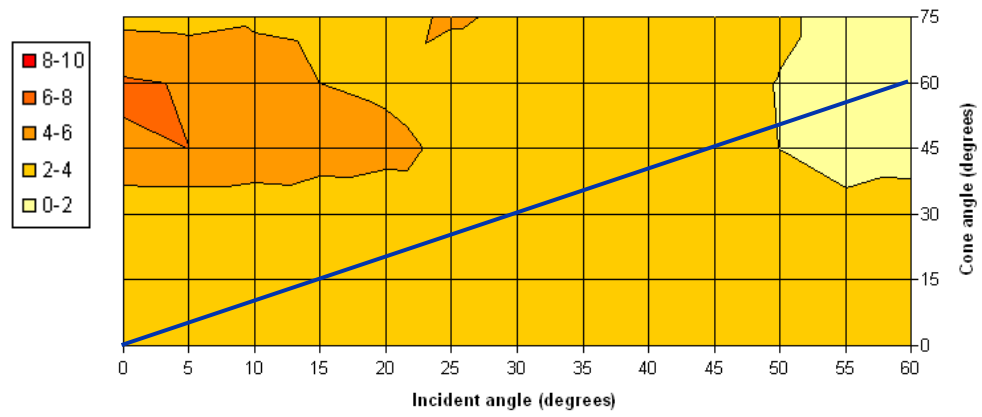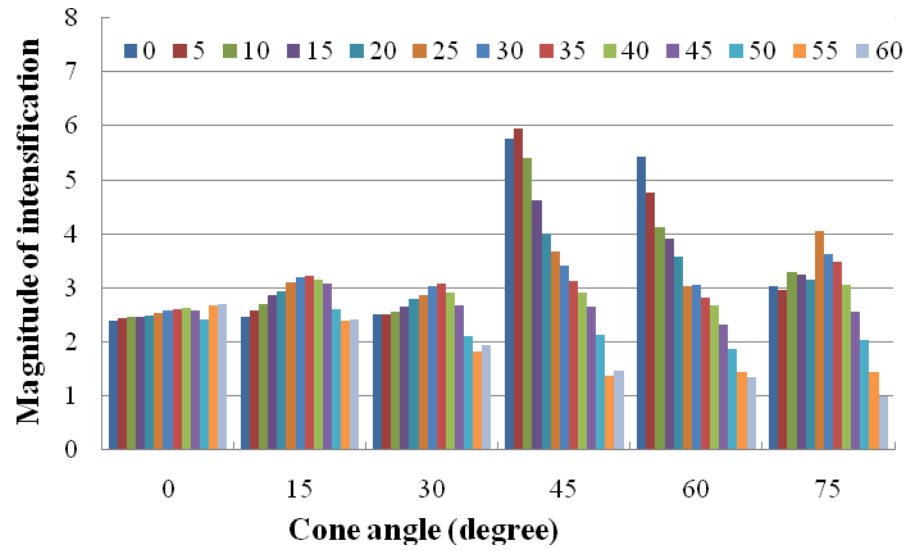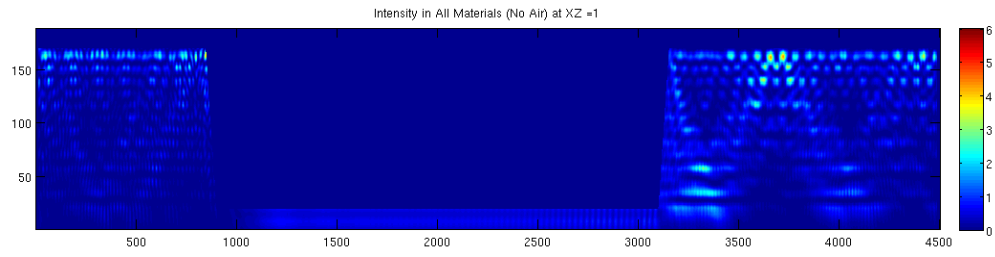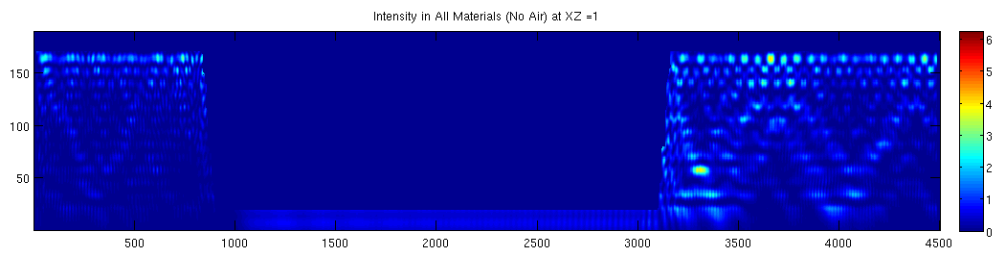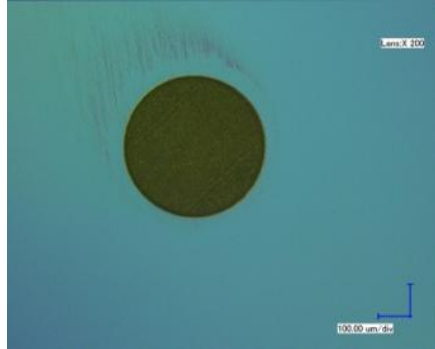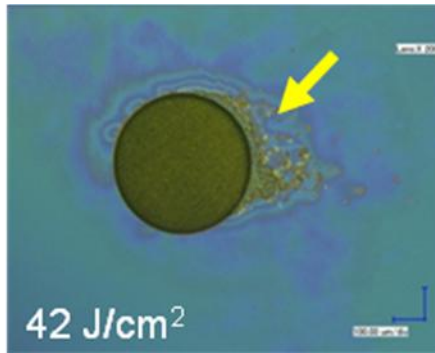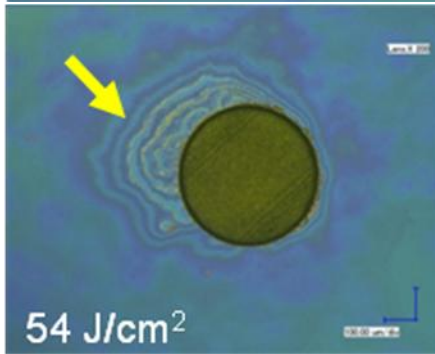
(c)

S polarization Imax = 3.6

42 J/cm^2

(d)

P polarization Imax = 2.6

54 J/cm^2